How to cite: *Angew. Chem. Int. Ed.* **2023**, *62*, e202215170
International Edition: doi.org/10.1002/anie.202215170
German Edition: doi.org/10.1002/ange.202215170

Main-Group Clusters

Low-Valent M_xAl_3 Cluster Salts with Tetrahedral $[SiAl_3]^+$ and Trigonal-Bipyramidal $[M_2Al_3]^{2+}$ Cores (M = Si/Ge)

*Philipp Dabringhaus, Silja Zedlitz, Luisa Giarrana, David Scheschkewitz, and Ingo Krossing**

Dedicated to Professor Hansgeorg Schnöckel and Professor Peter Jutzi

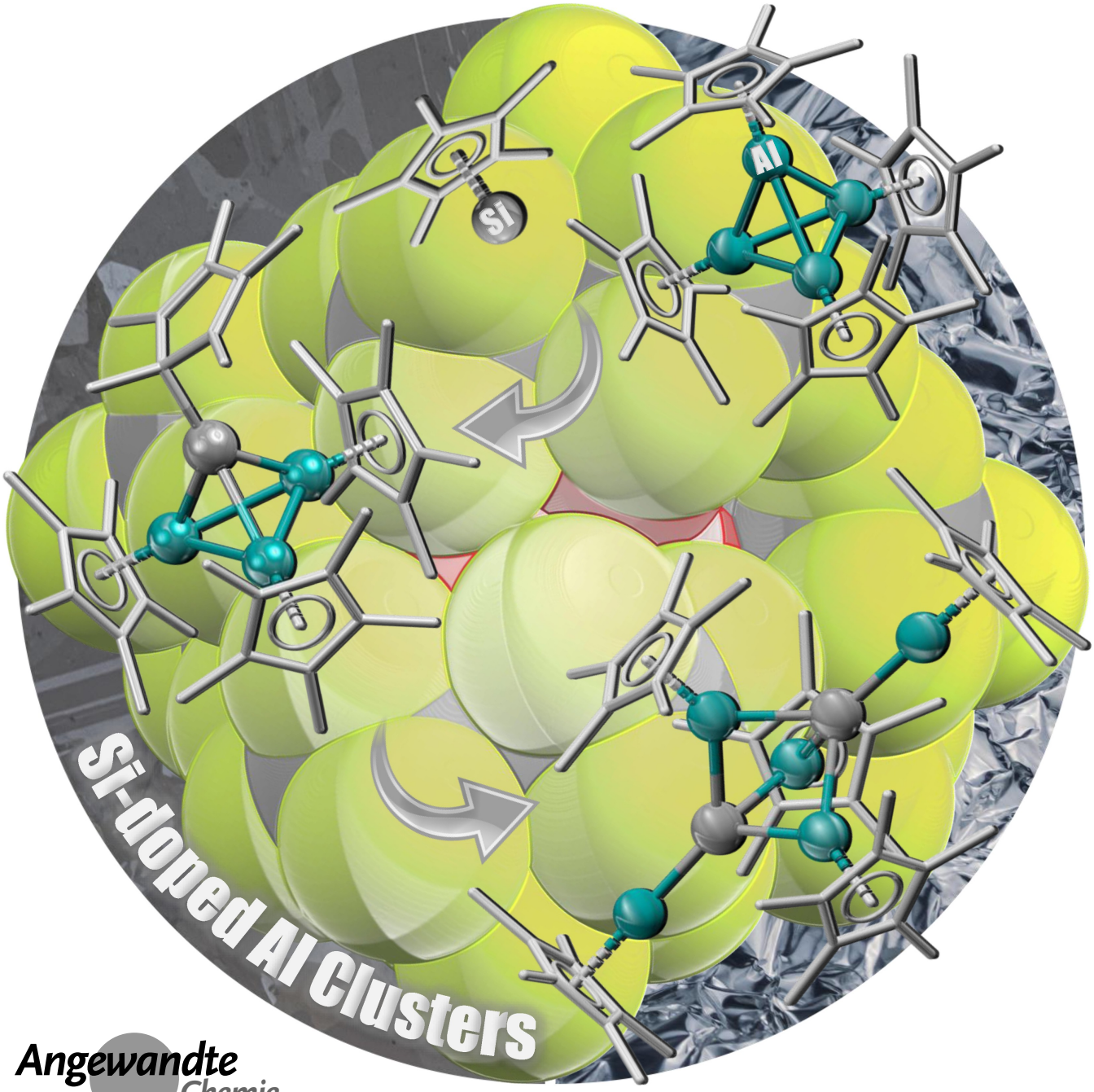

Abstract: Schnöckel's $[(AlCp^*)_4]$ and Jutzi's $[SiCp^*][B(C_6F_5)_4]$ ($Cp^* = C_5Me_5$) are landmarks in modern main-group chemistry with diverse applications in synthesis and catalysis. Despite the isoelectronic relationship between the AlCp* and the $[SiCp^*]^+$ fragments, their mutual reactivity is hitherto unknown. Here, we report on their reaction giving the complex salts $[Cp^*Si(AlCp^*)_3][WCA]$ ($[WCA]^- = [Al(OR^F)_4]^-$ and $[F\{Al(OR^F)_3\}_2]^-$; $R^F = C(CF_3)_3$). The tetrahedral $[SiAl_3]^+$ core not only represents a rare example of a low-valent silicon-doped aluminium-cluster, but also—due to its facile accessibility and high stability—provides a convenient preparative entry towards low-valent Si–Al clusters in general. For example, an elusive binuclear $[Si_2(AlCp^*)_5]^{2+}$ with extremely short Al–Si bonds and a high negative partial charge at the Si atoms was structurally characterised and its bonding situation analysed by DFT. Crystals of the isostructural $[Ge_2(AlCp^*)_5]^{2+}$ dication were also obtained and represent the first mixed Al–Ge cluster.

Introduction

Molecular silicon clusters have been heavily investigated due to promising applications ranging from small-molecule activation to the deposition of silicon as bulk and thin films.[1] Synthetic chemists have developed a library of structurally-diverse neutral and anionic, saturated and unsaturated silicon clusters. For example, saturated tetrasilatetrahedranes,[2] hexasilaprismanes,[3] and octasilacubanes[4] have been isolated, but also the unsaturated dismutational isomer of hexasilabenzene as well as the corresponding global minimum isomer.[5,6] The anionic congeners[7–9] constitute valuable starting materials for the incorporation of group 13 (B) and 15 (P) atoms into the silicon scaffold.[8] The atomically precise expansion of siliconoids[10] as well as germanium-substituted derivatives has been reported more recently.[11–13] In contrast, mixed cluster compounds with the similarly abundant metal aluminium, for which an extensive cluster chemistry has been developed separately,[14] are mostly restricted to the endohedral incorporation of silicon atoms. Jutzi and Schnöckel reported the synthesis of the unique $Si@Al_{14}Cp^*_6$ cluster containing a $Si@Al_8$ core (**I**),[15] which has since than also been observed in the analogous $Si@Al_{14}(N(Dipp)SiMe_3)_6$ cluster ($Dipp = 2,6\text{-}iPr_2C_6H_3$)[16] and, although distorted, in the superatomic $Si@Al_{56}[N(Dipp)SiMe_3]_{12}$ cluster (Scheme 1).[17] Other than these, only saturated Si–Al compounds including $SiAl_3$ (**II**) and $SiAl_4$ (**IV**) cores were hitherto reported.[18] The trigonal bipyramidal *closo*-Al_4Si cluster (**V**) synthesised by Schnöckel is the sole example with a silicon atom incorporated into the polyhedral aluminium scaffold.[19]

Although these structures **I–V** already hint to the diversity of assemblies possible in low-valent Si–Al clusters, a more detailed analysis of the bonding and especially follow-up chemistry is limited by the need for metastable AlX (X = Cl, Br, I) solutions as Al source in the synthesis of the above presented species. AlX solutions are typically prepared in situ in a highly specialised apparatus.[20] Due to the high reactivity of aluminium(I) halides, the products are often only prepared in low yields.

Hence, we were interested to synthesise low-valent Si–Al species in a systematic manner from accessible starting materials. Schnöckel's tetrahedral $[(AlCp^*)_4]$[21] (**VI**, $Cp^* = C_5Me_5$) and Jutzi's $[SiCp^*][B(C_6F_5)_4]$[22] (**VII**) are among the most prominent protagonists of low-valent main-group chemistry. Moreover, both molecules became more readily available in recent years[23] and are widely applied starting materials for low-valent Al and Si chemistry.[24,25] Yet, the mutual reaction between **VI** and **VII** has never been reported.

Here, we describe the synthesis and characterisation of complex salts with tetrahedral $[SiAl_3]^+$ cluster core stabilised by weakly-coordinating anions (WCAs) that were obtained from the reaction of $[SiCp^*][WCA]$ with $[(AlCp^*)_4]$ ($[WCA]^- = [Al(OR^F)_4]^-$ and $[F\{Al(OR^F)_3\}_2]^-$; $R^F = C(CF_3)_3$). Moreover, the formation of larger clusters featuring the dications $[M_2(AlCp^*)_5]^{2+}$ (M = Si, Ge) serves

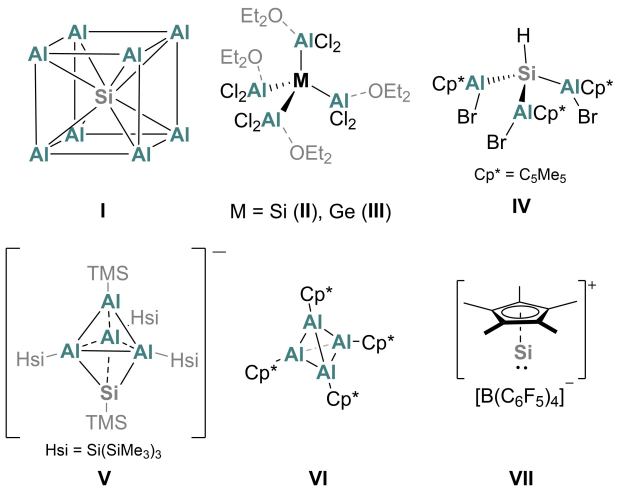

Scheme 1. Central $Si@Al_8$ unit discovered in large mixed clusters, literature known mixed low-valent Si–Al compounds as well as Schnöckel's $[(AlCp^*)_4]$ and Jutzi's $[SiCp^*]^+$. $Hsi = Si(SiMe_3)_3$; $TMS = SiMe_3$; $Cp^* = C_5Me_5$.

[*] P. Dabringhaus, S. Zedlitz, I. Krossing
Albert-Ludwigs-Universität Freiburg, Institute for Inorganic and Analytical Chemistry, Freiburg Materials Research Center FMF
Albertstraße 21, 79104 Freiburg i. Br. (Germany)
E-mail: krossing@uni-freiburg.de

L. Giarrana, D. Scheschkewitz
Chair in General and Inorganic Chemistry, Saarland University
66123 Saarbrücken (Germany)

as proof-of-principle demonstrating the potential to access larger mixed group 13/14 clusters starting from $[SiAl_3]^+$ precursors.

Results and Discussion

Syntheses and Basic Characterisation

The $[Al(OR^F)_4]^-$ salt of Jutzi's silicocenium cation, [SiCp*][$Al(OR^F)_4$] **1A**, was synthesised in 88 % yield in analogy to a known procedure via the reaction of $[H(Et_2O)_2][Al(OR^F)_4]$ with $SiCp^*_2$ (Scheme 2a).[26] The complex salt [SiCp*][F{Al(OR^F)$_3$}$_2$] **1B** with the even less coordinating [F{Al(OR^F)$_3$}$_2$]$^-$ anion was synthesised by abstraction of a Cp* ligand from $SiCp^*_2$ with the masked silylium agent $Me_3Si–F–Al(OR^F)_3$.[27] Addition of two equivalents of $Me_3Si–F–Al(OR^F)_3$ directly yielded the fluoride-bridged anion in **1B** with 87 % yield (Scheme 2b). The aluminate salts of the heavier germanocenium cation in [GeCp*][WCA] ([WCA]$^-$ = $[Al(OR^F)_4]^-$ (**2A**), [F{Al(OR^F)$_3$}$_2$]$^-$ (**2B**)) were synthesised by the analogous reaction routes (**2A** 88 % yield, **2B** 73 % yield, Scheme 2a/b). The complex salts were obtained as scXRD-quality crystals.[28] The bulk purity was confirmed NMR spectroscopically (Supporting Information, section 1). The compounds are stable at rt in the solid state and in 1,2-difluorobenzene (1,2-DFB) solution.

Mixed M-Al Clusters

Aiming for the isolation of a mixed Si–Al cluster, the silicocenium salts were each reacted with 0.75 equiv of [(AlCp*)$_4$] at −40 °C in 1,2-DFB. After 2 h, the formation of an orange solution was observed in both cases from which orange crystals were isolated upon crystallisation induced by layering the solution with *n*-heptane. scXRD analysis revealed the successful synthesis of the tetrahedral cluster cations $[Cp^*Si(AlCp^*)_3]^+$ as complex salts with $[Al(OR^F)_4]^-$ (**3A**, 59 % yield) or [F{Al(OR^F)$_3$}$_2$]$^-$ counterions (**3B** 77 % yield; Scheme 2c).[28]

Heating a solution of **3A** in 1,2-DFB for 10 h to 60 °C resulted in partial decomposition of the cluster. NMR spectroscopy revealed the formation of $[Al^{III}Cp^*_2]^+$, which suggests that Al^ICp^* disproportionates and acted as a reducing agent. Various other products were detected in the ^{1}H NMR spectrum (Supporting Information, Figure S32), but unfortunately not identified. Nonetheless, crystallisation yielded a few yellow crystals of the dicationic cluster $[Si_2(AlCp^*)_5]([Al(OR^F)_4])_2$ (**4**)[28] next to yellow powder and colourless crystals of $[AlCp^*_2][Al(OR^F)_4]$ (Scheme 2d). Similarly, a few crystals of **4** were obtained by the reaction of **3A** with Jones's $[Mg(NacNac^{Mes})]_2$ ($NacNac^{Mes}$ = $[(MesNCMe)_2CH]^-$ with Mes = 2,4,6-$(Me)_3C_6H_3$),[29] albeit next to various unidentifiable side products. In an analogous manner, yellow crystals of the germanium-analogue $[Ge_2(AlCp^*)_5]([Al(OR^F)_4])_2$ (**5**) were isolated from the reaction of **2A** with ¾ [(AlCp*)$_4$] at −40 °C,[28] which represents the first ever structurally characterised mixed Ge–Al cluster. In this case, the $[GeAl_3]^+$ tetrahedron, the plausible intermediate, could not be observed even at −40 °C. Similar to the synthesis of the silicon analogue **4**, the formation of $[Al^{III}(Cp^*)_2]^+$ was confirmed by NMR spectroscopy (Scheme 2f).

Molecular Structure and Spectroscopic Characterisation of the $SiAl_3^+$ Clusters

In the molecular structure of **3A**, a silyliumylidene-type $[Si(\eta^1\text{-}Cp^*)]^+$ cation has formally substituted an AlCp* unit in the starting material [(AlCp*)$_4$] (Figure 1a). Analysis of the structure of the cation in **3A** reveals barely significant elongation of the Al–Al bonds compared to Schnöckel's [(AlCp*)$_4$] tetrahedron ($d(Al–Al)_{avg.}$ = 2.769)[21] with values ranging from 2.769(2) Å to 2.816(2) Å ($d(Al–Al)_{avg.}$ = 2.798 Å). Moreover, the observed Si–C (d(Si–C) = 1.954 (4) Å/1.964(4) Å) and Si–Al bond lengths ($d(Si–Al)_{range}$ = 2.465(2)–2.522(2) Å, $d(Si–Al)_{avg.}$ = 2.485 Å) fit well to values observed for Si–C and Si–Al single bonds (cf. d((TMS)Si–Al) = 2.445(2) Å) in **V**).[19] The tetrahedron is compressed with larger Al–Si–Al angles ranging from 67.73(4)° to 69.42(4)° (∡(Al–Si–Al)$_{avg.}$ = 68.50) compared to Al–Al–Al angles (∡(Al–Al–Al)$_{range}$ = 59.95(4)° to 60.64(4)°, ∡(Al–Al–Al)$_{avg.}$ = 60.00°). Unfortunately, extensive disorder of the anions and cations in the molecular structure of **3B** precludes a detailed comparison of the bonding parameters.

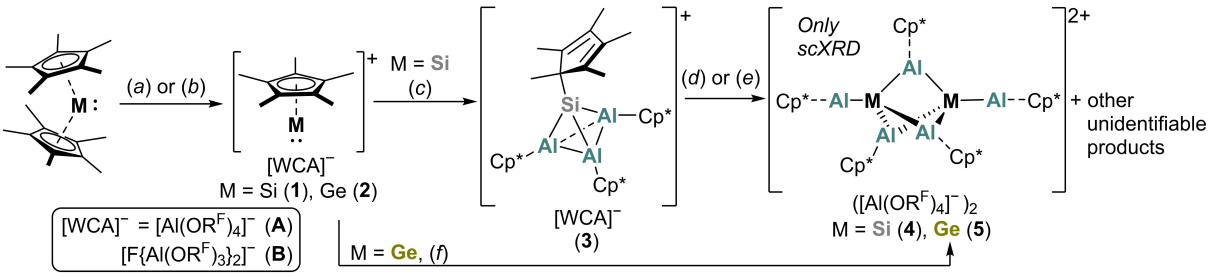

Scheme 2. Synthesis of novel aluminate salts of $[MCp^*]^+$ (M = Si, Ge) and formation of M–Al clusters upon addition of [(AlCp*)$_4$]. Reaction conditions: a) $[H(Et_2O)_2][Al(OR^F)_4]$, −Cp*H, PhF, −40 °C, 3 h; b) 2 $Me_3SiF–Al(OR^F)_3$, $–Me_3SiF$, $–Cp^*SiMe_3$, 1,2-DFB, rt, 3 h; c) ¾ [(AlCp*)$_4$], 1,2-DFB, −40 °C, 2 h; d) 1,2-DFB, 60 °C, 10 h, −[$AlCp^*_2$][$Al(OR^F)_4$]; (*e*) [Mg($NacNac^{mes}$)]$_2$, 1,2-DFB, rt, 5 min; f) ¾ [(AlCp*)$_4$], −[$AlCp^*_2$][$Al(OR^F)_4$], 1,2-DFB, rt, 5 min ; $NacNac^{Mes}$ = $[(MesNCMe)_2CH]^-$ with Mes = 2,4,6-$(Me)_3C_6H_3$.

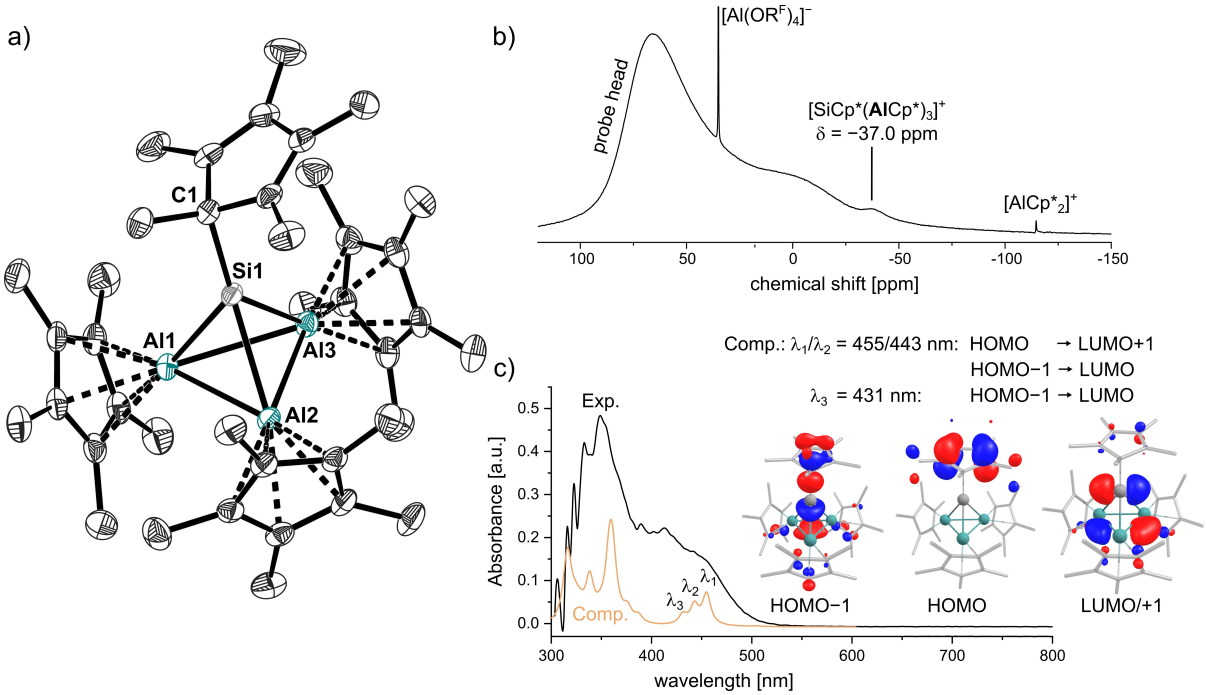

Figure 1. a) Molecular structure of the $[Cp^*Si(AlCp^*)_3]^+$ cation in **3A**. Hydrogen atoms and $[Al(OR^F)_4]^-$ anions omitted for clarity. Thermal displacement of the ellipsoids was set at 50% probability. b) ^{27}Al NMR spectrum (104.3 MHz, 1,2-DFB, 298 K) of **3A**. c) Experimental UV/Vis spectrum (1,2-DFB, rt) of **3A** compared to the theoretical UV/Vis spectrum of $[Cp^*Si(AlCp^*)_3]^+$ computed with TD-DFT at BP86-D3BJ/def2-SVP level of DFT. Moreover, molecular orbitals representing the ground states of the electronic transitions are displayed (isovalue 0.04).

Nevertheless, the connectivity of the $[SiAl_3]^+$ cluster can unambiguously be identified as the same as in **3A**.

NMR Spectra

The bulk purity of the products was confirmed by NMR and vibrational spectroscopy. In the ^1H NMR spectrum of **3A**/**3B**, sharp singlets for the protons of the AlCp* and $[SiCp^*]^+$ units are observed at 1.70 and 1.85 ppm. This observation points to a fluxional behaviour of the η^1-coordinated Cp* ligand at silicon, but suggests that any exchange of Cp* ligands between silicon and the aluminium centres is slow on the NMR time scale.[30] The ^{27}Al NMR resonance of the cationic part of **3A**/**3B** at −37.0 ppm is more low-field shifted compared to those of the related $[M(AlCp^*)_3]^+$ (M = Al, Ga, In, Tl)[25,31] as well as to $[(AlCp^*)_4]$ (Figure 1b). Moreover, the silicon atom gives rise to a signal at $\delta^{29}Si = +57.9$ ppm (cf. **1**: $\delta^{29}Si = -397.4$ ppm).

Raman Spectra

For compounds **3A**/**3B**, bands assigned to the stretching vibrations of the Si–Al bonds in the $SiAl_3$-cluster, the tetrahedral breathing modes, were detected at 454 cm^{-1} and 463/461 cm^{-1} (see Supporting Information, Figure S29). These values compare well to M–Al stretching vibrations reported for the cationic complexes of type $[M(AlCp^*)_3]^+$ (M = Al,[25] Ga-Tl[31]) but are higher compared to the Raman band of $[(AlCp^*)_4]$ ($\tilde{\nu} = 378\ cm^{-1}$). This indicates a higher strength of the M–Al bonds in the intermetallic compounds compared to the Al–Al bonds in tetrameric $[(AlCp^*)_4]$.

UV/Vis-Data

In accordance with the orange colour of **3A**, the UV/Vis spectrum of **3A** shows a broad shoulder between 400 and 500 nm (Figure 1c). In contrast, the broad UV/Vis bands of yellow $[(AlCp^*)_4]$ in 1,2-DFB do not absorb with significant intensity above 400 nm. TD-DFT computations assign the broad shoulder to electronic transitions from the HOMO centred at the η^1-Cp* ligand and HOMO-1 with lone-pair character at Si into the degenerate LUMO/+1 with p_x/p_y character at Si.

Bonding within the Tetrahedral $[SiAl_3]^+$ Cluster

EDA-NOCV-Analyses

Insight into the differences of the bonding interactions within the new and known tetrahedral clusters were gained by EDA-NOCV calculations (energy decomposition analysis with natural orbitals for chemical valence). Here, interactions of the aluminylene and silyliumylidene fragments with the $(AlCp^*)_3$ trimer were studied (Figure 2a). In $[(AlCp^*)_4]$, the EDA-NOCV yields an interaction energy of $\Delta E_{Int} = -61.2\ kcal\,mol^{-1}$ with an orbital contribution of $\Delta E_{Orb} =$

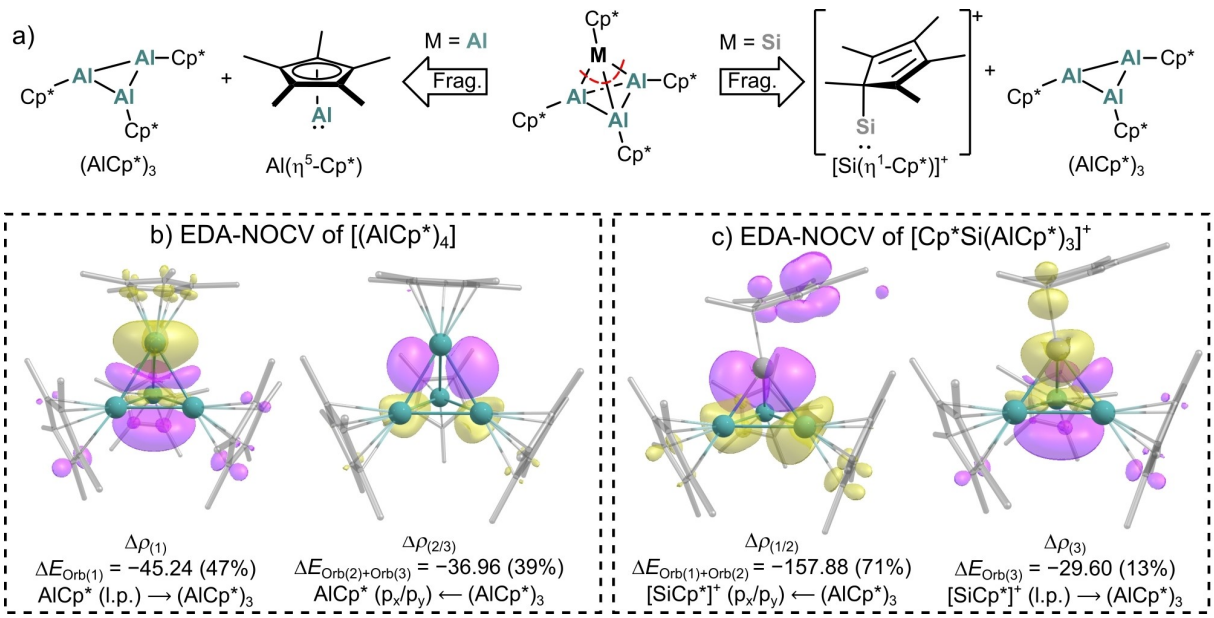

Figure 2. a) Fragmentation (Frag.) of the $[(AlCp^*)_4]$ and $[Cp^*Si(AlCp^*)_3]^+$ tetrahedra in the EDA-NOCV analysis into singlet (S) fragments. b) Plots of deformation density $\Delta\rho$ (isovalue 0.002) associated with the major contributing energy terms ΔE_{Orb} (values in kcal mol^{-1}) for fragmentation of $[(AlCp^*)_4]$ into AlCp* (S) and $(AlCp^*)_3$ (S). c) Plots of deformation density $\Delta\rho$ (isovalue 0.002) associated with the major contributing energy terms ΔE_{Orb} (values in kcal mol^{-1}) for fragmentation of $[Cp^*Si(AlCp^*)_3]^+$ into $[Si(\eta^1\text{-}Cp^*)]^+$ (S) and $(AlCp^*)_3$ (S). Charge flows from yellow to purple.

−95.5 kcal mol^{-1}. As visualised by the plots of the deformation densities, the orbital interaction is equally composed of a delocalisation of the AlCp* lone-pair orbital into the LUMO of the $(AlCp^*)_3$ fragment and the back donation of electron density from occupied ligand-group orbitals of $(AlCp^*)_3$ into empty p_x/p_y-orbitals at AlCp* (Figure 2b). The interaction energies, however, are more than doubled in the $[Cp^*Si(AlCp^*)_3]^+$ cluster ($\Delta E_{Int} = -143.1$ kcal mol^{-1}, $\Delta E_{Orb} = -222.7$ kcal mol^{-1}). In addition, the back donation of electron density from the $(AlCp^*)_3$ fragment into empty p orbitals at the silyliumylidene-type cation has become the major interaction, while the delocalisation of the lone pair at silicon represents only a minor interaction (Figure 2c). Overall, the orbital interaction becomes the dominating contribution to the total attractive interaction energy in the $[SiAl_3]^+$ cluster (60 %). In $[(AlCp^*)_4]$, the orbital interaction term contributes with only 41 % to the attractive interaction energy, with the rest representing dispersion forces (12 %) and electrostatic interactions (47 %).

A similar bonding interaction compared to $[Cp^*Si(AlCp^*)_3]^+$ was computed for the recently reported $[Al(AlCp^*)_3]^+$ cation,[25] although the interaction energies of the Al^+ cation with the $(AlCp^*)_3$ unit in $[Al(AlCp^*)_3]^+$ are considerably smaller compared to those in $[Cp^*Si(AlCp^*)_3]^+$.

QTAIM-Analyses

The high bond strength of the Si–Al bonds is also reflected in the QTAIM analysis (quantum theory of atoms in molecules). Here, the electron density ρ_r at the BCPs (bond critical point) of the Si–Al bonds averages to a value of 0.35 e$^-$ Å^{-3} (*cf.* Al–Al in $[(AlCp^*)_4]$: $\rho_{r,avg.} = 0.29$ e$^-$ Å^{-3}). In accordance with the scXRD analysis, the lower electron densities at the BCPs of the Al–Al bonds in $[SiAl_3]^+$ ($\rho_{r,avg.} = 0.23$ e$^-$ Å^{-3}) confirm the weakening of the Al–Al bonds. Intriguingly, the computed QTAIM charge at the silicon atom is significantly negative ($q_{Si} = -0.52$) while high positive charges are calculated for the Al atoms ($q_{Al,avg.} = +1.35$; $q_{AlCp^*,avg.} = -0.67$; cf. $[(AlCp^*)_4]$: $q_{Al,avg.} = 0.84$). Hence, a formal reduction of the silicon atom has occurred.

Molecular Structures with Trigonal Bipyramidal M_2Al_3 Core (M = Si, Ge)

Main-group metal-clusters with trigonal bipyramidal frameworks have been widely reported in group 14 in the homonuclear, heavier [1.1.1]propellane analogues.[32,33] Moreover, heteronuclear Ge_2Sn_3 and Ga_2Ge_3 cluster cores with formally bridging tetrylenes are known.[34] For group 13 metals, the structural motif can be found in clusters with alkali metals of type $M^1{}_2[(M^2R)_3]$ (M^1/M^2 = Na/Al,[35] Na/Ga,[36] K/Ga;[37] R = $Mes_2C_6H_3$), representing an aromatic $[M_3]^{2-}$ ring bicapped electrostatically by alkali-metal cations. Notably, similar structural motifs as the central $[M_2(AlCp^*)_3]$ cluster core in **4** and **5** were reported for the only other known main-group metal-AlCp* clusters (M = As,[38] Sb, Bi[39]). In the cluster cores of **4** and **5**, two group 14 metal atoms are connected by three bridging AlCp* units (Figure 3). Two AlCp* moieties are coordinated end-on at Si/Ge and cap the complex. The Si–Al bonds in the Si_2Al_3 core ($d(Si–Al_{brid.})_{avg.} = 2.467$ Å) are of similar length compared to Si–Al bonds in the tetrahedron **3**. Yet, the terminal Si–Al bonds are significantly shortened to 2.327(1) Å and repre-

sent to the best of our knowledge the shortest structurally characterised Si–Al bonds.

Similar differences of the bond lengths are observed in the Ge_2Al_5 cluster with short terminal Ge–Al bonds at 2.336(1)/2.334(2) Å. The Si–Si/Ge–Ge distances of 3.254(1) Å and 3.3055(9) Å are much longer than the corresponding distances between the naked Si/Ge atoms in the aforementioned benzpolarene and propellane motifs (2.55–2.78 Å),[5–12,33] which is in line with the expected absence of a bonding interaction in **4** and **5**.

Bonding within the Trigonal Bipyramidal M_2Al_3 Clusters (M = Si, Ge)

Just as the HOMO in the reported $[M_2(AlCp^*)_3]$ (M = As,[38] Sb, Bi[39]) clusters, the degenerate HOMO/-1 in **4** and **5** display Si/Ge-centered p orbitals (Figure 4a). Analysis of the molecular orbitals reveals the bonding in the M_2Al_3 cluster core to be best described as *closo*-Wade cluster. The six skeletal electron pairs (SEP) of the trigonal-bipyramidal Si_2Al_3 cluster (Figure 4b) match the SEPs computed for the

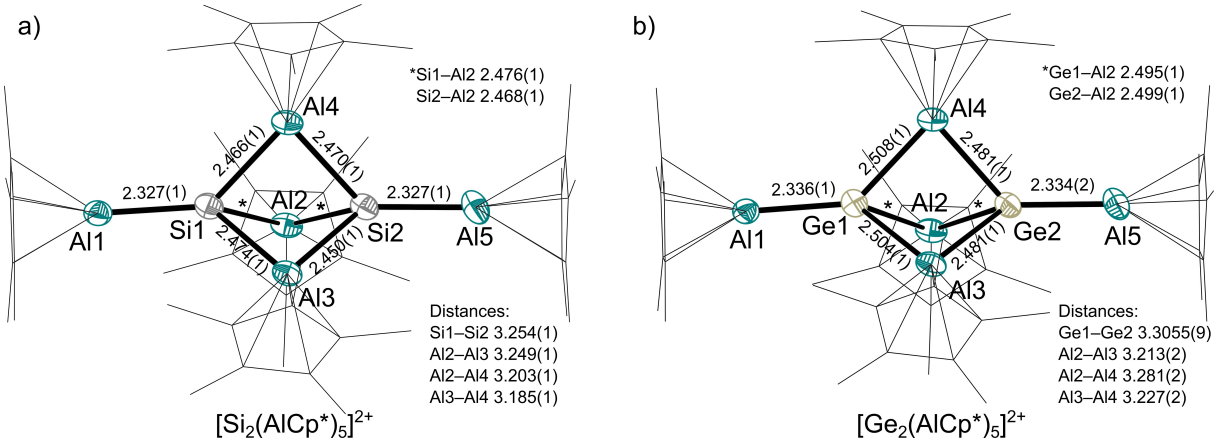

Figure 3. a) Molecular structure of the $[Si_2(AlCp^*)_5]^{2+}$ cation in **4**. Hydrogen atoms and $[Al(OR^F)_4]^-$ anions omitted for clarity. Thermal displacement of the ellipsoids was set at 50% probability. b) Molecular structure of the $[Ge_2(AlCp^*)_5]^{2+}$ cation in **5**. Hydrogen atoms and $[Al(OR^F)_4]^-$ anions omitted for clarity. Thermal displacement of the ellipsoids was set at 50% probability.

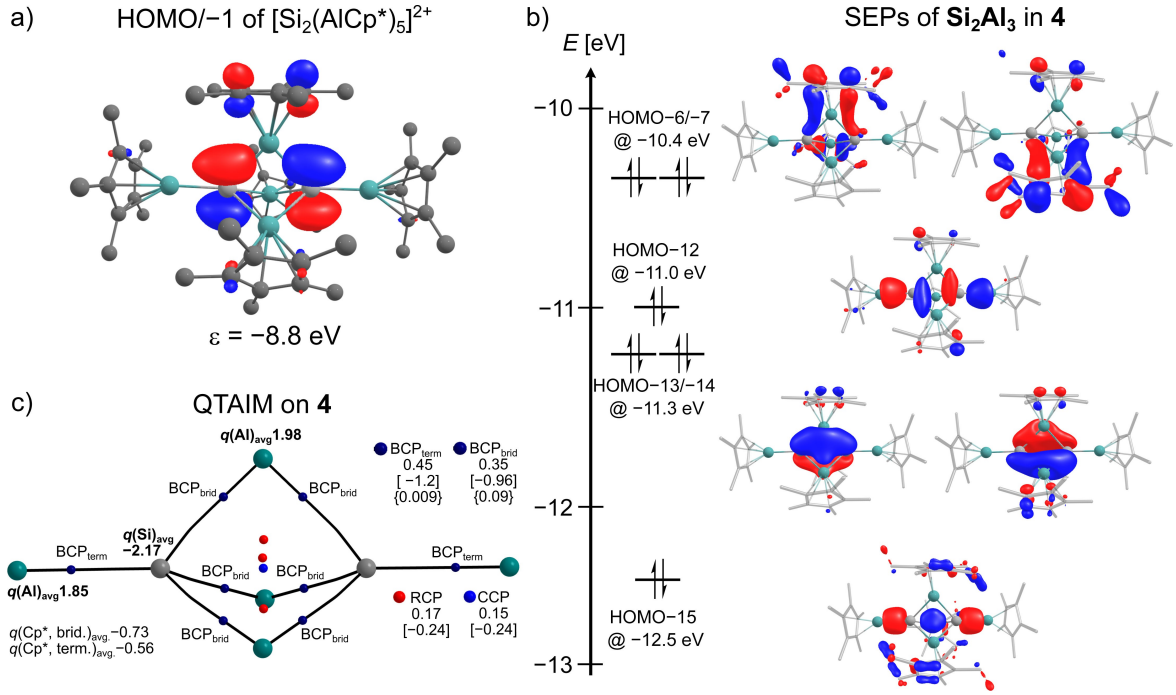

Figure 4. a) HOMO/−1 of *closo*-$[Si_2(AlCp^*)_5]^{2+}$ computed at the BP86-D3BJ/def2-SVP level of DFT (isovalue 0.04). b) Bonding skeletal orbitals SEPs (isovalue 0.03) of *closo*-$[Si_2(AlCp^*)_5]^{2+}$ computed at the BP86-D3BJ/def2-SVP level of DFT. c) Results of the QTAIM analysis for $[Si_2(AlCp^*)_5]^{2+}$ with average values for electron density ρ_r in $e^-Å^{-3}$ [Laplacian of electron density $\Delta\rho_r$ in $e^-Å^{-5}$] {bond ellipticity ε} at the critical points (BCP = bond critical points, RCP = ring critical point, CCP = cluster critical points).

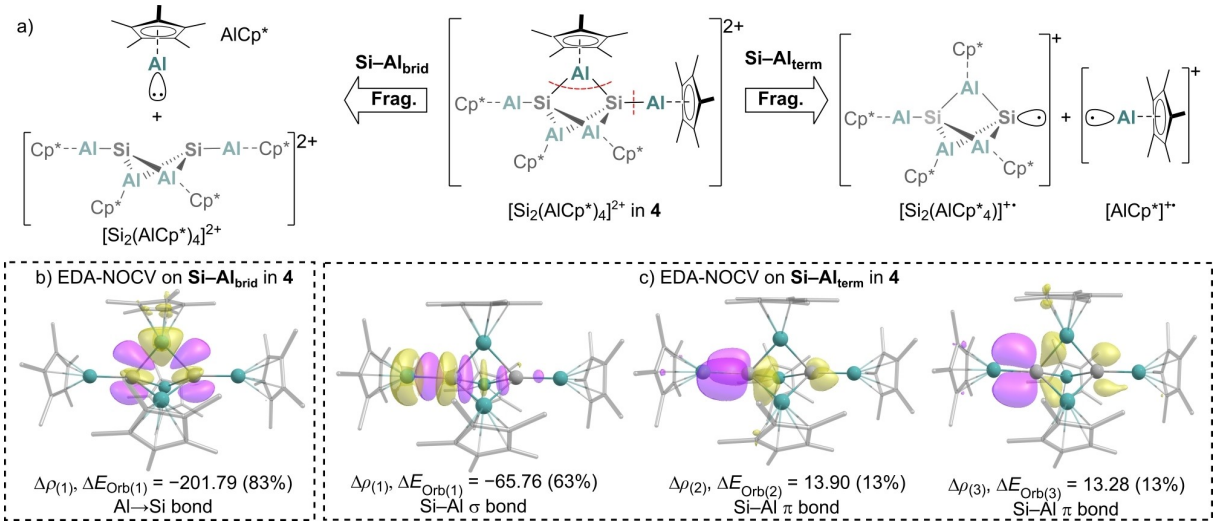

Figure 5. a) Fragmentation (Frag.) of the Si–Al bonds of the bridging and the terminal AlCp* units in **4** in the EDA-NOCV analysis into fragments. b) Plots of deformation density $\Delta\rho$ (isovalue 0.003) associated with the major contributing energy term ΔE_{Orb} (values in kcal mol^{-1}) for fragmentation of bridging Si–Al–Si bonds in AlCp* (S) and [Si$_2$(AlCp*)$_4$]$^{2+}$ (S) fragments. c) Plots of deformation density $\Delta\rho$ (isovalue 0.001) associated with the major contributing energy terms ΔE_{Orb} (values in kcal mol^{-1}) for fragmentation of terminal Al–Si bond in [AlCp*]$^{+}$ (D) and [Si$_2$(AlCp*)$_4$]$^{+}$ (D) fragments. Charge flows from yellow to purple.

model compound *closo*-[B$_5$H$_5$]$^{2-}$ (Supporting Information, Figure S46). However, the long Al–Al distances and the absence of BCPs in the QTAIM analysis exclude a strong covalent interaction between adjacent bridging Al atoms. SEPs and high electron density on ring critical points (RCPs) in Si$_2$Al$_3$ imply weakly bonding Al–Al interactions as expected for a *closo*-cluster (Figure 4c).

The high electron densities residing on the BCPs of terminal Al–Si bonds ($\rho_r = 0.45$ e$^-$ Å^{-3}) are consistent with the strong bonding interactions suggested by the short bond lengths. The low values for the bond ellipticities of $\varepsilon < 0.01$ at the BCPs of terminal Al–Si bonds indicate no anisotropy of the curvature of the electron density orthogonal to the bond, as found for single or triple bonds.[40] Moreover, even larger negative QTAIM charges at the Si atoms in **4** are computed as compared to the Si atom in **3**, while the Al atoms bear higher positive charges. Similarly, negative QTAIM charges are computed for the Ge atoms in **5** (Supporting Information, Figure S57).

EDA-NOCV-Analyses

To further investigate the bonding situation in **4**, the Si–Al bonds were studied by EDA-NOCV analyses (Figure 5; Supporting Information, section 2). For the bridging AlCp* units, only minimal differences in energy are computed for a heterolytic fragmentation into singlet or the alternative homolytic fragmentation into triplet fragments (heterolytic: $\Delta E_{Orb(1)} = -244.57$ kcal mol^{-1}, homolytic: $\Delta E_{Orb(1)} = -238.04$ kcal mol^{-1}, see Figure 5a and Table S5). For simplification, only the fragmentation into singlet fragments is discussed. Here, the donation of electron density from the lone pair at the AlCp* moiety into p orbitals at the silicon atoms represents the major orbital interaction. This observation fits the highly positive QTAIM charges at the bridging Al atoms as well as the computed HOMO/-1 of the complex.

Moreover, the exceptionally short terminal Al–Si bond lengths at only 2.327(1) Å (Si) and 2.335(2) Å (Ge) can be rationalised by EDA-NOCV analyses. Here, the homoleptic fragmentation into two doublet fragments is computed to be more meaningful (Figure 5a; Supporting Information, Table S4). In addition to the σ bonding interaction ($\Delta\rho_{(1)}$ in Figure 5c), delocalisation of electron density from the M$_2$Al$_3$ core and p orbitals of the other Si atom to the Al–Si bond results in two π-bonding interactions ($\Delta\rho_{(2)}$ and $\Delta\rho_{(3)}$ in Figure 5c). These results are supported by the low bond ellipticity of $\varepsilon = 0.009$ that results from the two almost equal, but orthogonal π-interactions and agrees with the high electron densities residing on the terminal Si–Al BCPs as calculated in the QTAIM analysis in Figure 4c.

Conclusion

The rational synthesis of the tetrahedral [Cp*Si(AlCp*)$_3$]$^+$ cluster stabilised with the weakly coordinating anions [Al(OR^F)$_4$]$^-$ and [F{Al(OR^F)$_3$}$_2$]$^-$ is reported. The cluster was obtained by reaction of the readily available corresponding [SiCp*]$^+$ salts with [(AlCp*)$_4$] in 1,2-difluorobenzene. EDA-NOCV and QTAIM analyses revealed a significantly higher stability of the cationic SiAl$_3^+$ cluster compared to the iconic neutral Al$_4$ cluster in [(AlCp*)$_4$]. Yet, the cluster appears to be only metastable, as the silicon atom in [SiAl$_3$]$^+$ bears a negative QTAIM charge and formation of the larger cluster [Si$_2$(AlCp*)$_5$]$^{2+}$ was observed upon heating, which is accompanied by further a reduction of the silicon atoms. In contrast, the homologous mixed [GeAl$_3$]$^+$ tetrahedron appears to be unstable towards disproportionation into larger, unidentifiable clusters of which the salt including the

$[Ge_2(AlCp^*)_5]^{2+}$ dication could be structurally characterised. Future research will focus on expanding the field of mixed Si–Al and Si–Ge clusters and exploring the follow-up chemistry of the straightforwardly accessible cationic $[SiAl_3]^+$ tetrahedron.

Acknowledgements

We thank the Fonds of the Chemical Industry FCI for a fellowship for Philipp Dabringhaus, the German Research Foundation (DFG) for the funding of projects KR2046/35-1 and SCHE906/4-4 as well as the Albert-Ludwigs-University Freiburg and Saarland University for supporting the work. Furthermore, we thank Manuel Schmitt for help with the quantum-chemical calculations. We acknowledge Harald Scherer and Fadime Bitgül for measurement of NMR spectra. Furthermore, the authors acknowledge support by the state of Baden-Württemberg through bwHPC and the DFG through grant no INST 40/575-1 FUGG (JUSTUS 2 cluster). Open Access funding enabled and organized by Projekt DEAL.

Conflict of Interest

There are no conflicts to declare.

Data Availability Statement

X-ray crystallographic data are available free of charge from the Cambridge Crystallographic Data Centre under the reference numbers CCDC 2209238 (**1A**), 2209239 (**1B**), 2210642 (**2A**), 2209240 (**2B**), 2209241 (**3A**), 2210870 (**3B**), 2210446 (**4**), and 2210639 (**5**). All other data supporting the findings are contained in the main text or the Supporting Information.

Keywords: Aluminium · Bond Theory · Cluster Compounds · Silicon · Weakly-Coording Anions

[1] a) Y. Heider, D. Scheschkewitz, *Chem. Rev.* **2021**, *121*, 9674; b) Y. Heider, D. Scheschkewitz, *Dalton Trans.* **2018**, *47*, 7104.
[2] N. Wiberg, C. M. M. Finger, K. Polborn, *Angew. Chem. Int. Ed. Engl.* **1993**, *32*, 1054; *Angew. Chem.* **1993**, *105*, 1140.
[3] a) K. Abersfelder, A. Russell, H. S. Rzepa, A. J. P. White, P. R. Haycock, D. Scheschkewitz, *J. Am. Chem. Soc.* **2012**, *134*, 16008; b) Y. Li, J. Li, J. Zhang, H. Song, C. Cui, *J. Am. Chem. Soc.* **2018**, *140*, 1219; c) A. Sekiguchi, T. Yatabe, C. Kabuto, H. Sakurai, *J. Am. Chem. Soc.* **1993**, *115*, 5853.
[4] a) H. Matsumoto, K. Higuchi, Y. Hoshino, H. Koike, Y. Naoi, Y. Nagai, *Chem. Commun.* **1988**, 1083; b) H. Matsumoto, K. Higuchi, S. Kyushin, M. Goto, *Angew. Chem. Int. Ed. Engl.* **1992**, *31*, 1354; *Angew. Chem.* **1992**, *104*, 1410; c) A. Sekiguchi, T. Yatabe, H. Kamatani, C. Kabuto, H. Sakurai, *J. Am. Chem. Soc.* **1992**, *114*, 6260.
[5] K. Abersfelder, A. J. P. White, H. S. Rzepa, D. Scheschkewitz, *Science* **2010**, *327*, 564.
[6] K. Abersfelder, A. J. P. White, R. J. F. Berger, H. S. Rzepa, D. Scheschkewitz, *Angew. Chem. Int. Ed.* **2011**, *50*, 7936; *Angew. Chem.* **2011**, *123*, 8082.
[7] P. Willmes, K. Leszczyńska, Y. Heider, K. Abersfelder, M. Zimmer, V. Huch, D. Scheschkewitz, *Angew. Chem. Int. Ed.* **2016**, *55*, 2907; *Angew. Chem.* **2016**, *128*, 2959.
[8] Y. Heider, P. Willmes, V. Huch, M. Zimmer, D. Scheschkewitz, *J. Am. Chem. Soc.* **2019**, *141*, 19498.
[9] Y. Heider, N. E. Poitiers, P. Willmes, K. I. Leszczyńska, V. Huch, D. Scheschkewitz, *Chem. Sci.* **2019**, *10*, 4523.
[10] K. I. Leszczyńska, V. Huch, C. Präsang, J. Schwabedissen, R. J. F. Berger, D. Scheschkewitz, *Angew. Chem. Int. Ed.* **2019**, *58*, 5124; *Angew. Chem.* **2019**, *131*, 5178.
[11] L. Klemmer, V. Huch, A. Jana, D. Scheschkewitz, *Chem. Commun.* **2019**, *55*, 10100.
[12] A. Jana, V. Huch, M. Repisky, R. J. F. Berger, D. Scheschkewitz, *Angew. Chem. Int. Ed.* **2014**, *53*, 3514; *Angew. Chem.* **2014**, *126*, 3583.
[13] Y. Heider, P. Willmes, D. Mühlhausen, L. Klemmer, M. Zimmer, V. Huch, D. Scheschkewitz, *Angew. Chem. Int. Ed.* **2019**, *58*, 1939; *Angew. Chem.* **2019**, *131*, 1958.
[14] a) A. Schnepf, H. Schnöckel, *Angew. Chem. Int. Ed.* **2002**, *41*, 3532; *Angew. Chem.* **2002**, *114*, 3682; b) H. Schnöckel, *Dalton Trans.* **2005**, *19*, 3131.
[15] A. Purath, C. Dohmeier, A. Ecker, R. Köppe, H. Krautscheid, H. Schnöckel, R. Ahlrichs, C. Stoermer, J. Friedrich, P. Jutzi, *J. Am. Chem. Soc.* **2000**, *122*, 6955.
[16] M. Huber, J. Hartig, K. Koch, H. Schnöckel, *Z. Anorg. Allg. Chem.* **2009**, *635*, 423.
[17] M. Huber, A. Schnepf, C. E. Anson, H. Schnöckel, *Angew. Chem. Int. Ed.* **2008**, *47*, 8201; *Angew. Chem.* **2008**, *120*, 8323.
[18] A. Purath, C. Dohmeier, E. Baum, R. Köppe, H. Schnöckel, *Z. Anorg. Allg. Chem.* **1999**, *625*, 2144.
[19] J. Vollet, G. Stösser, H. Schnöckel, *Inorg. Chim. Acta* **2007**, *360*, 1298.
[20] a) C. Dohmeier, D. Loos, H. Schnöckel, *Angew. Chem. Int. Ed. Engl.* **1996**, *35*, 129; *Angew. Chem.* **1996**, *108*, 141; b) M. Tacke, H. Schnoeckel, *Inorg. Chem.* **1989**, *28*, 2895.
[21] C. Dohmeier, C. Robl, M. Tacke, H. Schnöckel, *Angew. Chem. Int. Ed. Engl.* **1991**, *30*, 564; *Angew. Chem.* **1991**, *103*, 594.
[22] P. Jutzi, A. Mix, B. Rummel, W. W. Schoeller, B. Neumann, H.-G. Stammler, *Science* **2004**, *305*, 849.
[23] a) C. Ganesamoorthy, S. Loerke, C. Gemel, P. Jerabek, M. Winter, G. Frenking, R. A. Fischer, *Chem. Commun.* **2013**, *49*, 2858; b) P. Ghana, M. I. Arz, G. Schnakenburg, M. Straßmann, A. C. Filippou, *Organometallics* **2018**, *37*, 772.
[24] a) H. W. Roesky, S. S. Kumar, *Chem. Commun.* **2005**, *32*, 4027; b) O. Kysliak, H. Görls, R. Kretschmer, *Dalton Trans.* **2020**, *49*, 6377; c) E. Fritz-Langhals, *Org. Process Res. Dev.* **2019**, *23*, 2369; d) M. Fischer, S. Nees, T. Kupfer, J. T. Goettel, H. Braunschweig, C. Hering-Junghans, *J. Am. Chem. Soc.* **2021**, *143*, 4106.
[25] P. Dabringhaus, J. Willrett, I. Krossing, *Nat. Chem.* **2022**, *14*, 1151.
[26] P. Jutzi, A. Mix, B. Neumann, B. Rummel, H.-G. Stammler, *Chem. Commun.* **2006**, 3519.
[27] a) M. Schorpp, I. Krossing, *Chem. Eur. J.* **2020**, *26*, 14109; b) M. Rohde, L. O. Müller, D. Himmel, H. Scherer, I. Krossing, *Chem. Eur. J.* **2014**, *20*, 1218.
[28] Deposition Numbers 2209238 (for **1A**), 2209239 (for **1B**), 2210642 (for **2A**), 2209240 (for **2B**), 2209241 (for **3A**), 2210870 (for **3B**), 2210446 (for **4**), and 2210639 (for **5**) contain the supplementary crystallographic data for this paper. These data are provided free of charge by the joint Cambridge Crystallographic Data Centre and Fachinformationszentrum Karlsruhe Access Structures service.

[29] a) S. J. Bonyhady, C. Jones, S. Nembenna, A. Stasch, A. J. Edwards, G. J. McIntyre, *Chem. Eur. J.* **2010**, *16*, 938; b) S. P. Green, C. Jones, A. Stasch, *Science* **2007**, *318*, 1754.
[30] P. Jutzi, *Comments Inorg. Chem.* **1987**, *6*, 123.
[31] P. Dabringhaus, I. Krossing, *Chem. Sci.* **2022**, *13*, 12078.
[32] a) D. Nied, W. Klopper, F. Breher, *Angew. Chem. Int. Ed.* **2009**, *48*, 1411; *Angew. Chem.* **2009**, *121*, 1439; b) L. R. Sita, R. D. Bickerstaff, *J. Am. Chem. Soc.* **1989**, *111*, 6454; c) A. V. Protchenko, D. Dange, A. D. Schwarz, C. Y. Tang, N. Phillips, P. Mountford, C. Jones, S. Aldridge, *Chem. Commun.* **2014**, *50*, 3841; d) J. D. Erickson, J. C. Fettinger, P. P. Power, *Inorg. Chem.* **2015**, *54*, 1940.
[33] D. Nied, R. Köppe, W. Klopper, H. Schnöckel, F. Breher, *J. Am. Chem. Soc.* **2010**, *132*, 10264.
[34] A. F. Richards, M. Brynda, P. P. Power, *Organometallics* **2004**, *23*, 4009.
[35] R. J. Wright, M. Brynda, P. P. Power, *Angew. Chem. Int. Ed.* **2006**, *45*, 5953; *Angew. Chem.* **2006**, *118*, 6099.
[36] X.-W. Li, W. T. Pennington, G. H. Robinson, *J. Am. Chem. Soc.* **1995**, *117*, 7578.
[37] X.-W. Li, Y. Xie, P. R. Schreiner, K. D. Gripper, R. C. Crittendon, C. F. Campana, H. F. Schaefer, G. H. Robinson, *Organometallics* **1996**, *15*, 3798.
[38] C. K. F. von Hänisch, C. Üffing, M. A. Junker, A. Ecker, B. O. Kneisel, H. Schnöckel, *Angew. Chem. Int. Ed. Engl.* **1996**, *35*, 2875; *Angew. Chem.* **1996**, *108*, 3003.
[39] C. Ganesamoorthy, J. Krüger, E. Glöckler, C. Helling, L. John, W. Frank, C. Wölper, S. Schulz, *Inorg. Chem.* **2018**, *57*, 9495.
[40] C. Silva Lopez, A. R. de Lera, *Curr. Org. Chem.* **2011**, *15*, 3576.

Manuscript received: October 15, 2022
Accepted manuscript online: December 7, 2022
Version of record online: January 12, 2023